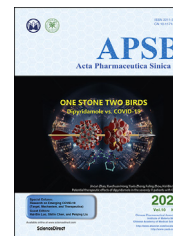Chinese Pharmaceutical Association
Institute of Materia Medica, Chinese Academy of Medical Sciences

Acta Pharmaceutica Sinica B

www.elsevier.com/locate/apsb
www.sciencedirect.com

ORIGINAL ARTICLE

Evaluation of ^{124}I-JS001 for hPD1 immuno-PET imaging using sarcoma cell homografts in humanized mice

Haifeng Huang[a,b,†], Hua Zhu[c,†], Quan Xie[a], Xiaobin Tian[a], Xianteng Yang[a,b], Fan Feng[d], Qiyu Jiang[d], Xinan Sheng[e,*], Zhi Yang[c,*]

[a]*Guizhou University School of Medicine, Guizhou University, Guiyang 550025, China*
[b]*Department of Orthopaedics, Guizhou Provincial People's Hospital, Guiyang 550002, China*
[c]*Key Laboratory of Carcinogenesis and Translational Research (Ministry of Education/Beijing), Department of Nuclear Medicine, Peking University Cancer Hospital & Institute, Beijing 100142, China*
[d]*Research Center for Clinical and Translational Medicine, the 302nd Hospital of Chinese PLA, Beijing 100039, China*
[e]*Key Laboratory of Carcinogenesis and Translational Research (Ministry of Education/Beijing), Department of Renal Cancer and Melanoma, Peking University Cancer Hospital & Institute, Beijing 100142, China*

Abstract JS001 (toripalimab) is a humanized IgG monoclonal antibody which strongly inhibits programmed cell death protein 1 (PD1). In this study, we used a different iodine isotype ($^{nat/124/125}$I) to label JS001 probes to target the human PD1 (hPD1) antigen. *In vitro*, the half maximal effective concentration (EC$_{50}$) value of ^{nat}I-JS001 did not significantly differ from that of JS001. The uptake of ^{125}I-JS001 by activated T cells was 5.63 times higher than that by nonactivated T cells after 2 h of incubation. The binding affinity of ^{125}I-JS001 to T cells of different lineages after phytohemagglutinin (PHA) stimulation reached 4.26 nmol/L. Humanized *PD1* C57BL/6 mice bearing mouse sarcoma S180 cell tumors were

Iodine isotopes

validated for immuno-positron emission tomography (immuno-PET) imaging. Pathological staining was used to assess the expression of PD1 in tumor tissues. The homologous [124]I-human IgG ([124]I-hIgG) group or blocking group was used as a control group. Immuno-PET imaging showed that the uptake in the tumor area of the [124]I-JS001 group at different time points was significantly higher than that of the blocking group or the [124]I-hIgG group in the humanized *PD1* mouse model. Taken together, these results suggest that this radiotracer has potential for noninvasive monitoring and directing tumor-specific personalized immunotherapy in PD1-positive tumors.

1. Introduction

In the past few years, checkpoint blockade therapy has shown impressive efficacy in the treatment of human cancer[1]. The clear benefits of this technique for patients are undeniable, and meet the need for long-awaited targeted therapies. However, due to the lack of response and reliable biomarkers in most patients, the full potential of these treatments has not been reached. Tumor cells can evade T cell immune surveillance through the programmed cell death protein 1 (PD1) axis, and PD1 plays a critical role in tumor immunotherapy. Targeting the PD1/programmed cell death ligand 1 (PDL1) immune checkpoint pathway has rapidly become a therapeutic strategy for an increasing number of malignant tumors. However, because patient responses to PD1 immunotherapy vary, only a subset of patients receives clinical benefits[2]. Therefore, it is necessary to increase the efficacy of immunotherapy, and additional methods to screen for patients that express relevant proteins are urgently needed. The expression of PD1, which is detected by immunohistochemistry (IHC) analysis, on immune cells is a good predictive biomarker of treatment responses to immunotherapy for many cancers. However, this method is not consistently successful, as antibodies, cut-off values and targets (tumor or microenvironment) can vary. IHC is a method for assessing the use of clinically validated predictive biomarkers for checkpoint inhibitor treatment responses in a limited number of clinical settings. However, IHC is poorly predictive in most cases. Moreover, this method is invasive, and pathological tissue must be obtained by biopsy or surgery. In contrast, molecular imaging enables the analysis of the whole tumor and metastases, thereby avoiding sampling errors and misunderstandings due to intra- and intertumoral heterogeneity. Molecular imaging enables the quantitative and longitudinal monitoring of PD1 expression without the need for repeated, invasive biopsies. Therefore, molecular imaging could potentially serve as a tool for monitoring PD1 expression or evaluating predictive biomarkers to select patients for immune checkpoint inhibitor (ICI) therapy during conventional anticancer treatments.

JS001, which is also known as toripalimab or TAB001, is a humanized IgG4 monoclonal antibody against PD1 that was approved by the National Medical Products Administration (NMPA) for immune therapy and can interact with human peripheral blood mononuclear cells (PBMCs). However, JS001 does not bind to the mouse PD1 antigen[3]. As a humanized IgG4 monoclonal antibody directed against the PD1 receptor, JS001 blocks the interaction of PD1 with its ligand and has been demonstrated to promote T cell activation in preclinical studies. Our previous research indicated that JS001 was well tolerated in patients, and no dose-limiting toxicity was observed[4].

Here, we report the generation of clinical grade [124]I-JS001 for evaluating human PD1 (hPD1) expression with immuno-positron emission tomography (immuno-PET) imaging in S180 homografts from humanized *PD1* C57BL/6 mice. We also demonstrate the potential of this noninvasive imaging technique for monitoring changes in hPD1 expression during malignant tumor cell proliferation. This study may provide a new strategy for guiding patient selection for hPD1 tumor immunotherapy.

2. Materials and methods

2.1. Materials and experimental animals

The JS001 monoclonal antibody and humanized *PD1* C57BL/6 male mice were provided by Shanghai Junshi Biosciences Co., Ltd. (Shanghai, China). Normal male C57BL/6 mice, male BALB/c nude mice and male Kunming mice were purchased from Beijing Huafukang Bioscience Co., Ltd. (Beijing, China). The mouse S180 sarcoma cell line was purchased from Beijing Zhongke Quality Inspection Biotechnology Co., Ltd. (Beijing, China). The human OS-732 cell line was purchased from the Institute of Cancer, Chinese Academy of Medical Sciences (Beijing, China). Normal peripheral blood T cells and CD3^{+} pan T cells were obtained from AllCells (PB009-1F-C, Emeryville, CA, USA). Phytohemagglutinin (PHA) and lectin from *Phaseolus vulgaris* were obtained from Sigma (L4144, St. Louis, MO, USA). Human IgG (IgG1) was purchased from Rongsheng Company (Shanghai, China). [124]I-I$_2$ was produced at the Beijing Cancer Hospital (370 kBq/μL dissolved in 0.02 mol/L NaOH) using the HM-20 cyclotron. Details regarding the materials are provided in the Supporting Information.

All procedures in studies involving animals were performed in accordance with the ethical standards of the institutional and/or national research committee. This study was approved by the Ethics Committee of the Peking University Cancer Hospital & Institute (Beijing, China), and informed consent was obtained.

2.2. [nat]I-JS001 production and physicochemical property assays

After the addition of 200 μL of phosphate buffer (0.1 mol/L, pH 7.0) to 1 mg (20 mg/mL) of JS001, K[nat]I solution was added at a $100 \times$ excess molar ratio. Next, 10 μL of *N*-bromosuccinimide (NBS, 1 mg/mL, pH 7.0) was added to the reaction for 60 s, followed by purification with a PD-10 column. The average molecular mass of JS001 before and after modification was determined with matrix-assisted laser desorption/ionization time-of-flight mass spectrometry (MALDI-TOF-MS). The binding

properties of JS001 and ^{nat}I-JS001 to the PD1 receptor were determined with direct ELISA, and the specific details of the experimental method are provided in the Supporting Information.

2.3. Radiolabeling and quality control of ^{124}I-JS001

The ^{124}I-JS001 labeling method is described in the Supporting Information (the labeling methods were similar for $^{125/131}$I-JS001). The stability of ^{124}I-JS001 in 5% human serum albumin (HSA) and phosphate buffered saline (PBS, pH7.0) was measured by radio-thin-layer chromatography (radio-TLC) at 2, 24, 48 and 72 h.

2.4. In vitro cell binding affinity and uptake assay

CD3$^+$ T cells were purchased from AllCells and were analyzed by flow cytometry. The expression of hPD1 in CD3$^+$ T cells after PHA stimulation was measured by Western blotting and flow cytometry, and additional details are provided in the Supporting Information. Further analysis of the binding abilities of JS001 and ^{nat}I-JS001 to the hPD1 receptor after T cell activation was conducted by flow cytometry. The cell uptake and affinity of CD3$^+$ T cells for these tracers after PHA stimulation were measured with in vitro cell uptake experiments. CD3$^+$ T cells that were not stimulated by PHA were used as negative controls.

Cell uptake experiment: T cells were plated in two 24-well plates at 3×10^5 cells/well ($n = 4$), and the experimental and control groups were divided into groups 1, 2, 3, and 4. The competitive inhibition group was divided into groups 5 and 6. In the competitive inhibition groups, 20 μg of JS001 was added for 2 h, and 74 kBq ^{125}I-JS001 was subsequently added to each well. The experimental and control groups were sampled at 10, 30, 60, and 120 min (for groups 1–4), respectively. Groups 5 and 6 were incubated for 60 and 120 min, respectively. The cells were washed twice with 1 mL of 0.1 mol/L PBS (pH 7.4), followed by centrifugation and resuspension. Finally, the radioactivity of each well was measured.

Dissociation constant (K_d) value determination: 6 groups of 4 wells were set up in 24-well plates. Plates were seeded with 6×10^5 T cells per well, and varying concentrations of ^{125}I-JS001 (3.7, 18.5, 37, 185, 370, and 740 kBq in 20 μL of PBS) were added to each well. After incubation for 240 min, cells were washed twice with 1 mL of PBS (pH 7.4), and the radioactivity counts were subsequently measured.

2.5. Tumor xenograft/homograft mouse models

Mouse S180 sarcoma and human OS-732 cells (5×10^6/group) were harvested in the logarithmic growth phase. Normal C57BL/6 male mice and humanized PD1 C57BL/6 male mice were inoculated with mouse S180 sarcoma cells, and BALB/c nude male mice were inoculated with human OS-732 cells, in the right axilla. Tumor-bearing model mice were housed in specific pathogen-free (SPF) conditions, and tumor diameters were regularly measured using a vernier caliper. After the tumor diameter reached 0.8–1.0 cm, the relevant in vivo experimental study was performed.

2.6. PCR and Western blot analyses of tumor tissue

After harvesting S180 tumor tissues from normal C57BL/6 mice, humanized PD1 C57BL/6 mice and OS-732 mice, total RNA was extracted, and PCR (polymerase chain reaction) was used to detect hPD1 gene expression in tumors. The forward hPD1 primer was 5′-GTGTCACACAACTGCCCAAC-3′, and the reverse primer was 5′-GCTCTCTTTGATCTGCGCCT-3′. The forward primer for mouse GAPDH was 5′-TTGCTGTTGAAGTCGCAG-3′, and the reverse primer was 5′-TGTGTCCGTCGTGGATCTT-3′. The expression of hPD1 in S180 tumor tissues from humanized PD1 C57BL/6 mice was measured by Western blotting. Additional details are provided in the Supporting Information.

2.7. Immuno-PET imaging

Three days prior to the injection of the radiotracer, the thyroid glands of KM mice were blocked by administering a 5‰ KI solution via their drinking water[5]. For each humanized PD1 C57BL/6 mouse with a S180 sarcoma tumor, 18.5 MBq ^{124}I-JS001 was injected through the tail vein ($n = 3$). Mice in the ^{124}I-human IgG (^{124}I-hIgG) group were injected with 18.5 MBq ^{124}I-hIgG ($n = 3$), and mice in the blocking group were coinjected with 18.5 MBq ^{124}I-JS001 and 500 μg of JS001 ($n = 3$). At each time point after injection, the tumor-bearing mice were anesthetized with 1.5% isoflurane and were placed in the prone position near the center of the field of view of a PET scanner (Sedecal, Spain); 10-min static scans were subsequently obtained. The images were reconstructed with a two-dimensional ordered subsets expectation maximum (OSEM) algorithm. Regions of interest (ROIs) were used to estimate the uptake of the radiotracer in each organ.

2.8. Pathological analysis

IHC analysis was performed to confirm the expression of human CD3 and hPD1 in S180 and OS-732 tumor tissues. Hematoxylin and eosin (HE) staining was performed to examine the S180 tumor tissue. Additional details are provided in the Supporting Information.

2.9. Statistical analysis

Data are presented as mean ± SD (standard deviation), and a t-test was used to analyze differences between two groups. The original 9.0 software was used to process data and images. Statistical analysis was performed with SPSS (SPSS, version 17.0; Chicago, IL, USA). P-values < 0.05 were considered statistically significant.

3. Results

3.1. ^{124}I-JS001 quality control and in vitro stability tests

A schematic diagram of the JS001-labeled isotope ^{124}I is provided in Supporting Information Fig. S1. The quality control data for ^{124}I-JS001 are shown in Supporting Information Table S1. The average radiochemical yield was 85% ($n = 5$). After purification,

the radiochemical purification yield was greater than 98%, and the specific activity was 450 MBq/nmol. As shown in Supporting Information Fig. S2, free ^{124}I was not found in the final product, ^{124}I-JS001, which was confirmed by radio-TLC. Radio-high-performance liquid chromatography (Radio-HPLC) showed that the UV (ultraviolet) peak retention time of JS001 was 5.24 min, and the radioactive peak retention time of ^{124}I-JS001 was 5.89 min (Fig. S2). Clinically relevant quality control indicators are shown in Table S1. The stability test of ^{124}I-JS001 *in vitro* provided promising results. The radiochemical purity of ^{124}I-JS001 was greater than 95% in PBS and was greater than 96% in 5% HSA after 72 h at 37 °C (Supporting Information Fig. S3).

3.2. ^{nat}I-JS001 activity analysis

The average molecular weight of JS001 was 149,670 Da based on MALDI-TOF-MS. After modification with ^{nat}I, the average molecular weight of ^{nat}I-JS001 was 150,847 Da, and approximately 9 ^{nat}I molecules were connected to JS001 (Fig. 1A and B). The EC_{50} value of JS001 was 0.89 ± 0.15 ng/mL, and the EC_{50} value of ^{nat}I-JS001 was 1.03 ± 0.14 ng/mL, which were not statistically significantly different from each other ($t = -1.68$, $P > 0.05$; Fig. 1C and D).
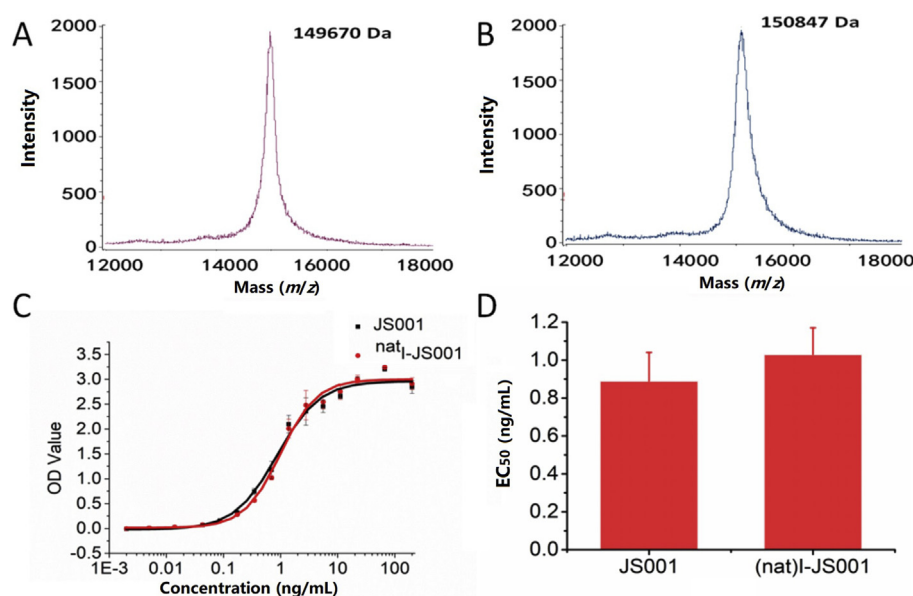
3.3. In vitro experiments

$CD3^{+}$ T cells were identified by flow cytometry. The fluorescence intensities of CD3 receptors on T cells before and after PHA stimulation (2 μg/mL for 3 day) were significantly different from those in the control group (Supporting Information Fig. S4A). hPD1 expression was upregulated in T cells after PHA stimulation (Fig. S4B). The fluorescence intensities of JS001 and ^{nat}I-JS001 for hPD1 receptors on T cells after PHA stimulation were significantly higher than those in the control group (Fig. S4C). The
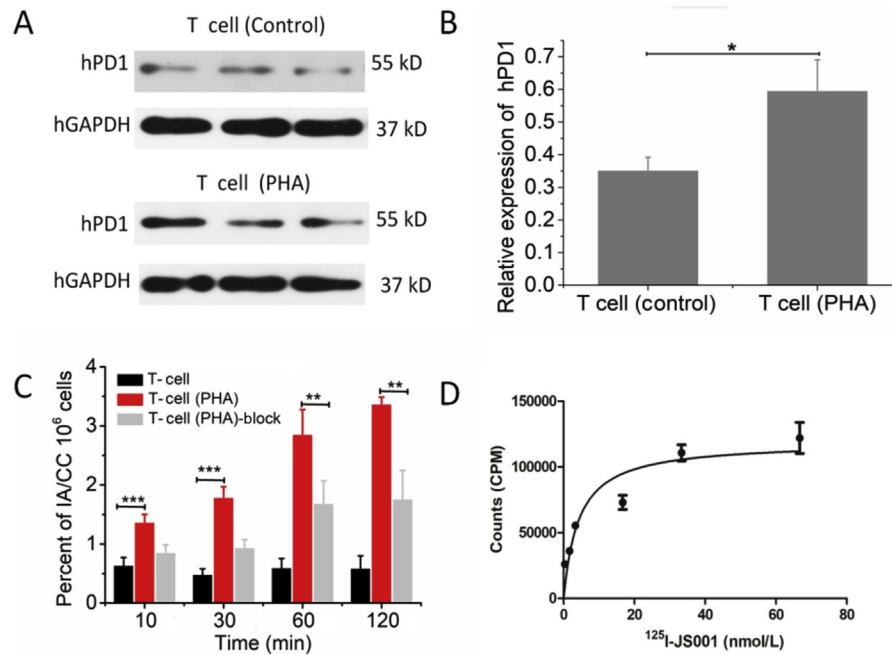
expression of hPD1 in T cells was measured by Western blotting with GAPDH used as internal standard. The relative expression level of hPD1 in T cells before PHA stimulation was 0.35 ± 0.04, but 0.60 ± 0.09 after PHA stimulation ($t = -4.16$, $P < 0.05$), indicating that hPD1 expression was upregulated in T cells after PHA stimulation (Fig. 2A and B). The cellular uptake rate of ^{125}I-JS001 in T cells (%IA/CC 10^{6} cells, %IA/CC: percent of collected count of total added count per mL) after PHA stimulation was significantly higher than that before stimulation, and the differences were statistically significant (10 min: 0.65 ± 0.13 *vs.* 1.37 ± 0.13, $t = -8.32$, $P < 0.001$; 30 min: 0.49 ± 0.09 *vs.* 1.79 ± 0.17, $t = -13.49$, $P < 0.001$). After blocking with JS001, the uptake value in T cells was significantly reduced at 60 and 120 min (60 min: 2.86 ± 0.41 *vs.* 1.69 ± 0.37, $t = 4.21$, $P < 0.01$; 120 min: 3.38 ± 0.11 *vs.* 1.77 ± 0.48, $t = 6.48$, $P < 0.01$; Fig. 2C). The ability of ^{125}I-JS001 to target hPD1 in T cells after PHA stimulation was assessed. Based on the cell binding affinity experiment, the K_{d} value was 4.26 nmol/L (Fig. 2D).

3.4. PCR and Western blot assays

The tumor tissues of humanized *PD1* C57BL/6 mice were analyzed by PCR, and the *hPD1* gene was detected (Fig. 3A). Results from gel analysis confirmed that the *hPD1* gene fragment was 125 bp (Fig. 3B). The cycle quantification (Cq) value of the *hPD1* gene was 27.8, and the Cq of the mouse *GAPDH* gene was 12.2. After the PCR amplification product was sequenced, the DNA sequence was confirmed in the NCBI database. The tumor tissues were analyzed by Western blotting, which indicated that the hPD1 receptor was present in tumor tissues (Fig. 3C). The gray value ratio of the hPD1 and mouse GAPDH proteins was 0.57 ± 0.14. The *hPD1* gene was not detected in the tumor tissues of normal C57BL/6 mice or nude mice (Supporting Information Figs. S5 and S6).

Figure 1 ^{nat}I modification of JS001. (A) Average molecular weight of JS001 as measured by MALDI-TOF-MS before the modification (149,670 Da). (B) Average molecular weight of ^{nat}I-JS001 as measured by MALDI-TOF-MS after the ^{nat}I modification (150,847 Da). (C) Comparison of the binding ability of JS001 to the hPD1 receptor before and after ^{nat}I labeling (ELISA). (D) There was no significant change in the EC_{50} values of JS001 for binding the hPD1 receptor before and after ^{nat}I labeling (results are shown as mean $\pm$ SD, $n = 6$; t-test, $P > 0.05$).

Figure 2 *In vitro* analyses of ^{125}I-JS001. (A) Protein expression of hPD1 and the internal reference human GAPDH in T cells before and after PHA stimulation (Western blotting). (B) Upregulation of hPD1 expression in T cells after PHA stimulation (results are shown as mean $\pm$ SD, $n = 3$; t-test, $^*P < 0.05$). (C) The radioactive uptake of ^{125}I-JS001 in T cells after PHA stimulation. The radioactive uptake of ^{125}I-JS001 in T cells was significantly reduced after blocking (results are shown as mean $\pm$ SD, $n = 4$; t-test, $^*P < 0.05$; $^{**}P < 0.01$; and $^{***}P < 0.001$). (D) The affinity of ^{125}I-JS001 in T cells; the K_d value is 4.26 nmol/L.
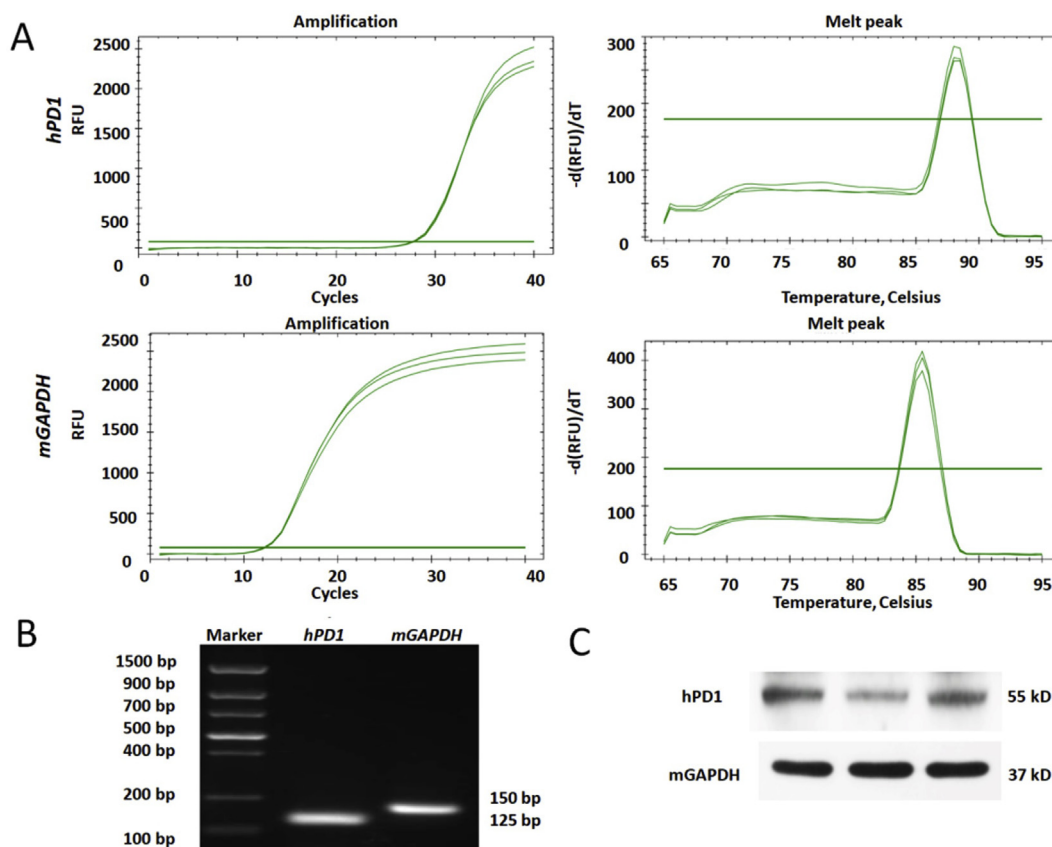
3.5. Immuno-PET imaging

For imaging, 18.5 MBq ^{124}I-JS001 or ^{124}I-hIgG was injected into the mice *via* the tail vein. Immuno-PET images of S180 homografts in humanized *PD1* C57BL/6 mice were obtained at different time points (2, 24, 48 and 72 h) (Fig. 4A−D). Due to the rapid growth of mouse S180 tumors, significant necrotic liquefaction occurred in the central region of the tumor. Because the tumors grew too fast, the mice had poor body condition and died 72 h after imaging. The standard uptake value (SUV) ratios of T/NT in these mouse groups gradually increased over time (Fig. 4E). We used classical blocking or homologous hIgG as a control, and immuno-PET imaging was performed at 4, 24, and 60 h after the injection of 18.5 MBq ^{124}I-JS001, 18.5 MBq ^{124}I-JS001 and 500 μg of JS001 (blocking group), or 18.5 MBq ^{124}I-hIgG. The probe uptake values at the tumor sites of the control groups (blocking group or ^{124}I-hIgG group) were lower than those at the tumor sites of the test group (Fig. 5A−C). The longest imaging time of ^{124}I-JS001 was 90 h (Supporting Information Fig. S7). The T/M (tumor/muscle) ratios at each time point after ^{124}I-JS001, ^{124}I-JS001 and JS001, or ^{124}I-hIgG injection were significantly different (Fig. 5D). The immuno-PET imaging of human OS-732 xenografts in nude mice was performed after the injection of 18.5 MBq ^{124}I-JS001, and no differences were observed in tumors that were imaged at different time points (2, 24, 48 and 72 h) (Fig. 6A and B). This finding was consistent with the results of the IHC staining of tumor hPD1 (Fig. 6D). The increase in the T/NT values over time may have been due to the EPR (enhanced permeability and retention) effect of the tumor (Fig. 6C). This imaging result further validated the specific affinity of ^{124}I-JS001 for the hPD1 receptor.

3.6. Pathological analysis

The CD3 receptor is a surface marker of mature T lymphocytes and is expressed in most T lymphocytes, while hPD1 is expressed in T cells that are activated by the tumor microenvironment. Comparing the IHC images of CD3 and hPD1, the positive staining areas of the two images were extremely similar, which demonstrated that hPD1 was mainly expressed in the CD3-positive area (Fig. 4F and G). HE staining confirmed that a significant necrotic, liquefied region appeared in the center of the S180 tumor (Fig. 4H and H1). IHC staining showed that there was no hPD1 expression in the tumor tissues of nude mice (Fig. 6D), which was consistent with the imaging results.

4. Discussion

Blockade of the interaction between PD1 and PDL1 by tumor immunotherapy antibodies has shown impressive efficacy in cancer patients. Immunotherapy has completely changed the long-term standard of care for cancer patients. For example, immunotherapeutic methods, such as immunological checkpoint blockade, are increasingly used for cancer treatment either alone or in combination with chemotherapy or radiation therapy[6]. Immunotherapy has shown good antitumor activity; in particular, PD1/PDL1 and cytotoxic T lymphocyte-associated antigen 4 (CTLA4) checkpoint inhibitors have altered tumor immune responses in small-cell lung cancer (SCLC), which has high immunogenicity, a high mutation load and other favorable immune factors. Thus, immunological checkpoint inhibitors may represent an important breakthrough in SCLC therapy[7]. In non-
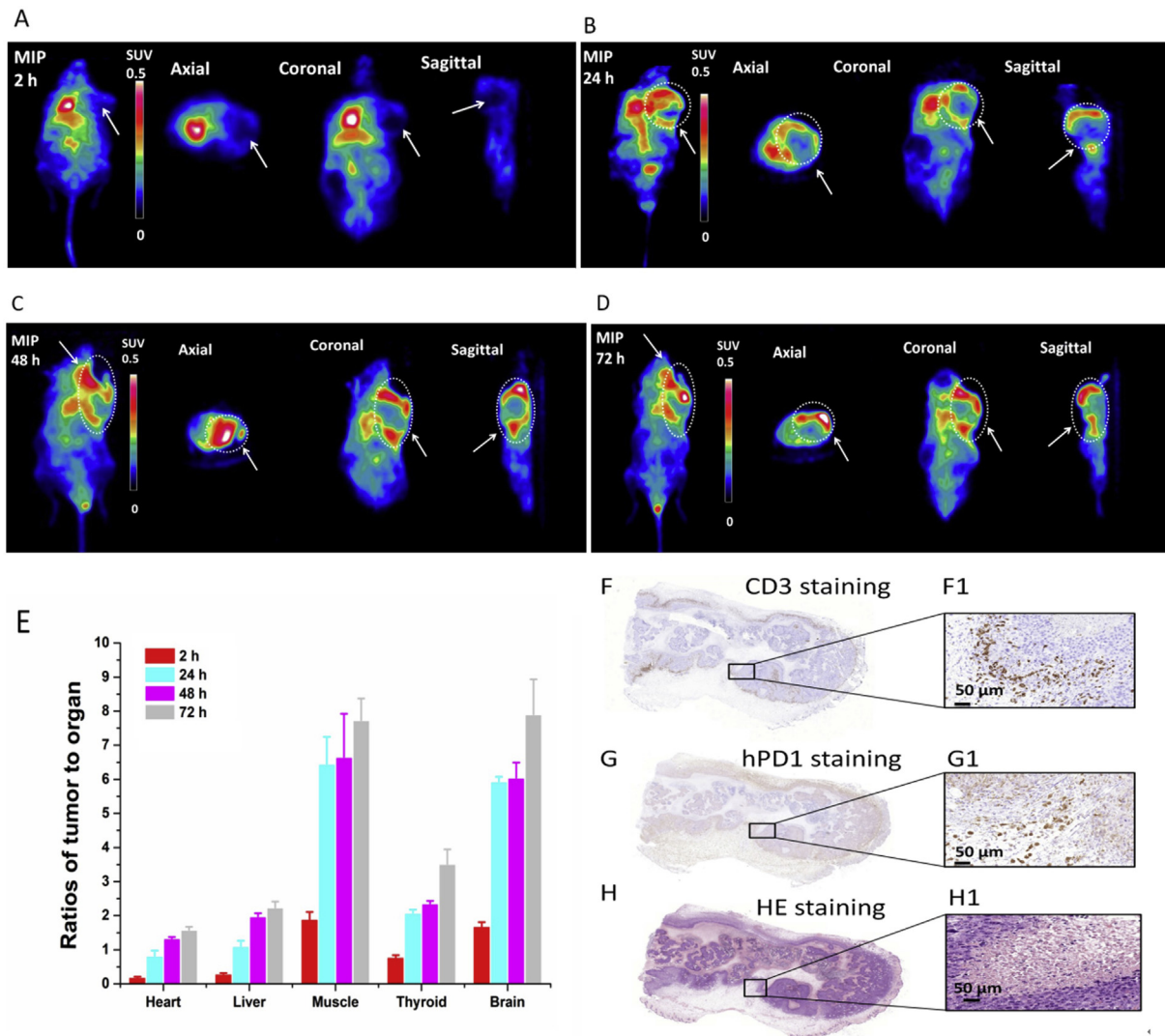
Figure 3 Identification of the hPD1 receptor in the tumor tissues of humanized *PD1* C57BL/6 mice. (A) The inflection points of the h*PD1* and mouse *Gapdh* gene amplification curves were clear, and the index periods were obvious. (B) The results from a gel showed that the amplified product corresponded to the fragment size of the hPD1 target gene, which was 125 bp. (C) The hPD1 receptor was expressed in tumor tissues.

small-cell lung cancer patients treated with immunological checkpoint inhibitors, the overall response rate that was confirmed during treatment was 21.1%[8]. Significant advances in the understanding of the pathophysiology of melanoma have led to a new era of melanoma treatment with targeted therapies and immunotherapy[9]. Despite the initial success of immunotherapy, molecular testing is urgently needed to determine whether patients are likely to respond. Studies on the ultrasensitivity of circulating tumor DNA (ctDNA) and T cell expansion for evaluating immune checkpoint blockade in patients with metastatic lung cancer have been reported in the literature[10]. Moreover, anti-PD1 antibodies have shown satisfactory results in the treatment of certain types of lymphoma[11]. However, PD1 is heterogeneously expressed within the tumor microenvironment, and its expression may change during disease progression and treatment.

It is very important to develop new methods for the direct, noninvasive and whole-body evaluation of PD1 expression in patients who could potentially receive anti-PD1 therapy, and the imaging analysis of PD1 could aid in patient selection. In recent years, studies have reported ^{89}Zr-, ^{64}Cu- and ^{111}In-labeled PD1/PDL1 imaging probes, in which labeled PD1/PDL1 monoclonal antibodies have been used in clinical studies and have generated good imaging results[12-16]. However, ^{111}In can only be imaged with SPECT (single-photon emission computed tomography), and the half-life of ^{64}Cu is shorter than the half-life of ^{124}I. The PD1 receptor could be visualized for up to 90 h after injection

in this study (Supporting Information Fig. S8). The half-life of ^{89}Zr is similar to that of ^{124}I, and both of these tracers are suitable for antibody evaluations. However, the lack of bifunctional chelators [only deferoxamine (DFO) is currently commercially available], longer incubation times, critical labeling conditions and, in some cases, antibody aggregation make ^{89}Zr difficult to use. The ^{124}I labeling method uses *in situ* labeling, does not require bifunctional chelators, and is simple and convenient.

Our previous research indicated that JS001 was well tolerated in patients, and no dose-limiting toxicity was observed. We hypothesized that the PET radionuclide iodine (^{124}I) could label JS001 to facilitate the detection of PD1 *in vivo*, and we evaluated the potential clinical utility of ^{124}I-JS001 as a PET imaging probe for the noninvasive screening of hPD1 expression in tumors. In this study, we compared the activities of JS001 and ^{nat}I-JS001, and demonstrated that the ^{nat}I label did not significantly affect the EC_{50} value of JS001. This finding indicates that the *in situ* ^{nat}I label has little effect on the activity of this antibody. The upregulation of hPD1 expression in T cells after PHA stimulation was shown by both Western blotting and flow cytometry. The uptake of ^{125}I-JS001 by T cells after PHA activation was significantly higher than that by non-activated T cells and could be blocked by the JS001. The ^{125}I-JS001 probe had high affinity *in vitro*, and the K_d value was 4.26 nmol/L. We constructed a S180 tumor model using humanized *PD1* C57BL/6 mice. hPD1 expression in this humanized tumor model, verified *via* PCR and Western blotting, was
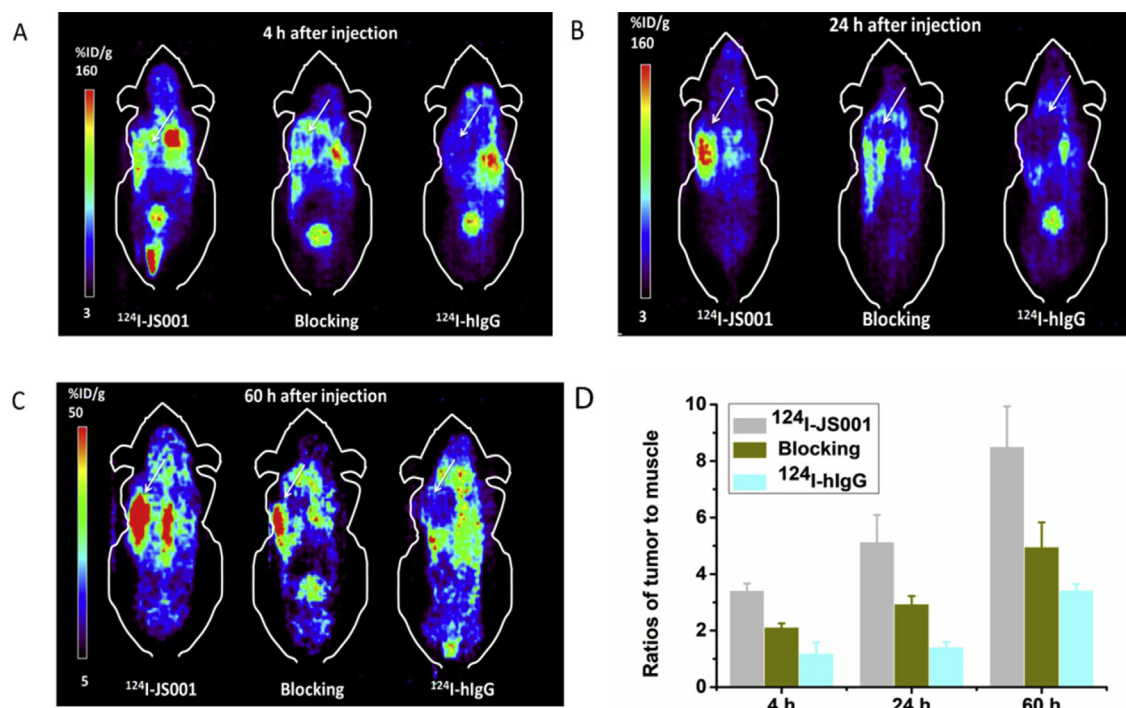
Figure 4 Immuno-PET imaging of S180 homografts in humanized *PD1* C57BL/6 mice after the injection of ^{124}I-JS001 (the arrow indicates the tumor). (A) Immuno-PET imaging at 2 h after 18.5 MBq ^{124}I-JS001 injection. (B) Immuno-PET imaging at 24 h after 18.5 MBq ^{124}I-JS001 injection. (C) Immuno-PET imaging at 48 h after 18.5 MBq ^{124}I-JS001 injection. (D) Immuno-PET imaging at 72 h after 18.5 MBq ^{124}I-JS001 injection. (E) T/NT SUV ratios at each time point after the injection of ^{124}I-JS001. (F) IHC staining of CD3 in S180 tumor tissue. (F1) CD3 expression in S180 tumors. (G) IHC staining of hPD1 in S180 tumor tissue. (G1) hPD1 expression in S180 tumor tissue. (H) HE staining of S180 tumor tissue. (H1) HE staining of an area of S180 tumor tissue.
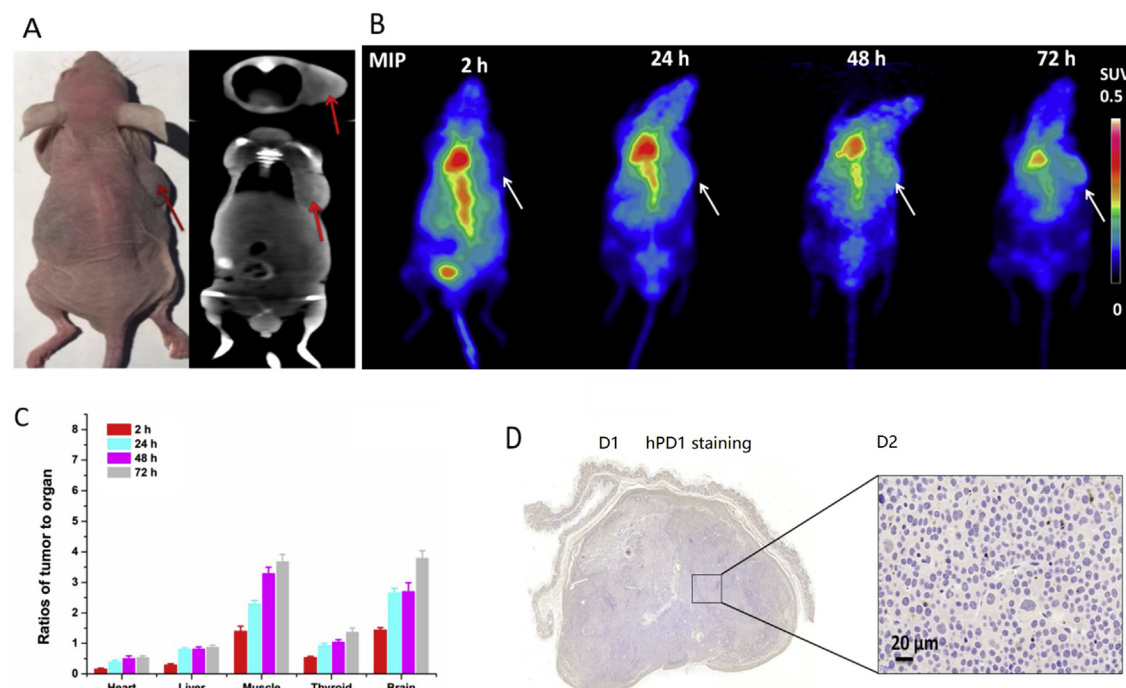
compared with that in nonhumanized tumor-bearing mice. Clear images were obtained in the tumor area 24 h after ^{124}I-JS001 injection. Although a large amount of liquefaction and necrosis occurred in the tumor area (due to rapid proliferation of S180 tumors) the ^{124}I-JS001 probe was able to detect the expression of hPD1 in the corresponding proliferative tumor area (Fig. 4A−D). Immuno-PET imaging was performed after the injection of probe (18.5 MBq ^{124}I-JS001 and 500 μg of JS001, 18.5 MBq ^{124}I-JS001 or 18.5 MBq ^{124}I-hIgG), and the probe uptake in the blocking group and the ^{124}I-hIgG group was lower than that in the ^{124}I-JS001 group. In addition, the tumor area was not visible at 4, 24, and 60 h after the injection of ^{124}I-hIgG (Fig. 5A−C). Throughout the entire imaging period, the tumor uptake of the ^{124}I-JS001 radiotracer was significantly higher than that of ^{124}I-hIgG, and the classic blocking pathway was also effective, which indicates that ^{124}I-JS001 specifically targets the hPD1 receptor

(Fig. 5D). Nude mice do not have a thymus and have almost no T cells. Because S180 tumors grow fast, the nude mice pass away quickly; thus, we chose to use other tumor-bearing mice for reimaging. Tumor imaging was negative at each different time points after the injection of ^{124}I-JS001 in nude mice with OS-732 tumors. No obvious signals were observed in the tumor area, also was consistent with the IHC staining of hPD1 in the tumors (Fig. 6D). These results demonstrate that the ^{124}I-JS001 molecular probe specifically targets the hPD1 receptor. The metabolism and bio-distribution of ^{131}I-JS001 is shown in Fig. S7.

Important functions of the immune system include detection of "foreign" *vs.* healthy cells, coordinating attacks on the former, and protection of the latter. Checkpoint inhibitors are considered the most important molecules in this process. Sarcomas are difficult to study due to their rarity and histomorphological complexity. PD1/PDL1 inhibitors have shown promising

Figure 5 Immuno-PET imaging of S180 homografts in humanized *PD1* C57BL/6 mice after the injection of [124]I-JS001 and [124]I-hIgG (the arrow indicates the tumor). The blocking group was coinjected with 18.5 MBq [124]I-JS001 and 500 μg of JS001. Immuno-PET imaging at 4 h (A), 24 h (B), and 60 h (C) after 18.5 MBq [124]I-JS001 and [124]I-hIgG injections. (D) Ratio in the ROI (T/M) at each time point after the injection of [124]I-JS001 and [124]I-hIgG.

Figure 6 Immuno-PET imaging of human OS-732 xenografts in nude mice after the injection of 18.5 MBq [124]I-JS001 (the arrow indicates the tumor). (A) OS-732 tumor inoculated on the right side of a nude mouse. (B) Immuno-PET imaging at each time point after 18.5 MBq [124]I-JS001 injection; no imaging of tumor tissue was observable. (C) T/NT SUV ratios at each time point after the injection of 18.5 MBq [124]I-JS001. (D) IHC staining of hPD1 in nude OS-732 tumor tissue; no hPD1 expression was observed, consistent with the previous tumor imaging result. (D1) Negative hPD1 expression region in the tumor tissue.

antitumor effects in solid tumors, such as sarcoma[17]. Although some patients show a complete and/or long-lasting response to ICI therapy, it is not possible to reliably predict patient responses. Thus, there is a need for validated robust biomarkers to overcome the challenge of predicting patient responses to ICI therapy[18]. We previously described a study of ^{99m}Tc-conjugated JS001[19]. JS001 labeled with ^{99m}Tc requires SPECT imaging, and the image resolution is worse than that of ^{124}I-labeled JS001. The ^{124}I labeling method uses *in situ* labeling and can be completed in one step, whereas ^{99m}Tc labeling is divided into two parts (JS001 to JS001-SH and JS001-SH to ^{99m}Tc-JS001), so the labeling of ^{124}I is simple and convenient. Because of the half-life (^{124}I has a half-life of approximately 4.2 days, and ^{99m}Tc has a half-life of approximately 6.02 h), the tumor imaging time of ^{99m}Tc-JS001 is also shorter than that of ^{124}I-JS001. In the present study, our tumor imaging was maintained for up to 90 h after injection, whereas in the previous study, the labeling was maintained for only 28 h after injection. However, compared with that of ^{124}I-JS001, the use of ^{99m}Tc-conjugated JS001 reduced the amount of radiation to the animal, which is convenient for animal body management. Furthermore, the IHC staining of humanized mouse tumor tissues confirmed the expression of hPD1, and the IHC analyses of CD3 and hPD1 were basically consistent (Fig. 4G).

Monoclonal antibodies are widely used because of their high specificity and ability to recognize a wide range of antigens[20]. Our most recent clinical trials demonstrated that the combination of JS001 with axitinib (a vascular endothelial growth factor inhibitor) showed promising antitumor activity in metastatic mucosal melanoma[21]. As a first-line treatment for metastatic mucosal melanoma, the objective response rate reached 48.3%, and this treatment method is expected to become the new international standard for the first-line treatment of mucosal melanoma. In this study, using nuclear medicine technology, we aimed to noninvasively detect the expression of PD1 in patients, thereby increasing their response rates to ICI therapy. The current situation is rapidly evolving, and new immunotherapy combination trials can further improve outcomes and evaluate predictive biomarkers to help identify the patients who are most likely to benefit from these therapies. Taken together, these results demonstrate that the ^{124}I-JS001 probe combined with PET imaging may be an important tool for the clinical screening of PD1-positive patients for tumor immunotherapy.

5. Conclusions

We produced and evaluated ^{124}I-JS001 for the noninvasive detection of hPD1. The ^{124}I-JS001 probe exhibited a high binding affinity that was comparable to JS001, and ^{125}I-JS001 had a high affinity for T cells stimulated by PHA. We showed that the micro-PET imaging signal corresponded to PD1 expression at tumor tissue sites of humanized *PD1* C57BL/6 mice. ^{124}I-JS001 showed potential for specifically targeting hPD1, which may provide a new strategy for guiding patient selection for hPD1 tumor immunotherapy.

Acknowledgments

Author contributions

Conflicts of interest

The authors declare that no competing interests exist regarding this study.

Appendix A.   Supporting information

Supporting data to this article can be found online at https://doi.org/10.1016/j.apsb.2020.02.004.

References

1. Filipska M, Pedraz-Valdunciel C, Chaib I, Rosell R. Biological therapies in lung cancer treatment: using our immune system as an ally to defeat the malignancy. *Expet Opin Biol Ther* 2019;**19**:457−67.
2. Havel JJ, Chowell D, Chan TA. The evolving landscape of biomarkers for checkpoint inhibitor immunotherapy. *Nat Rev Canc* 2019;**19**:133−50.
3. Fu J, Wang F, Dong LH, Zhang J, Deng CL, Wang XL, et al. Preclinical evaluation of the efficacy, pharmacokinetics and immunogenicity of JS-001, a programmed cell death protein-1 (PD-1) monoclonal antibody. *Acta Pharmacol Sin* 2017;**38**:710−8.
4. Tang B, Yan X, Sheng X, Si L, Cui C, Kong Y, et al. Safety and clinical activity with an anti-PD-1 antibody JS001 in advanced melanoma or urologic cancer patients. *J Hematol Oncol* 2019;**12**:7.
5. Wang F, Liu T, Li L, Guo X, Duan D, Liu Z, et al. Production, quality control of next-generation PET radioisotope iodine-124 and its thyroid imaging. *J Radioanal Nucl Chem* 2018;**318**:1999−2006.
6. Wirsdörfer F, de Leve S, Jendrossek V. Combining radiotherapy and immunotherapy in lung cancer: can we expect limitations due to altered normal tissue toxicity?. *Int J Mol Sci* 2018;**20**:E24.
7. Yu T, Zhong D. Clinical development of immunotherapy for small cell lung cancer. *Zhongguo Fei Ai Za Zhi* 2018;**21**:918−23.
8. Tachihara M, Negoro S, Inoue T, Tamiya M, Akazawa Y, Uenami T, et al. Efficacy of anti-PD-1/PD-L1 antibodies after discontinuation due to adverse events in non-small cell lung cancer patients (HANSHIN 0316). *BMC Cancer* 2018;**18**:946.
9. Sun J, Zager JS, Eroglu Z. Encorafenib/binimetinib for the treatment of BRAF-mutant advanced, unresectable, or metastatic melanoma: design, development, and potential place in therapy. *OncoTargets Ther* 2018;**11**:9081−9.

10. Anagnostou V, Forde PM, White JR, Niknafs N, Hruban C, Naidoo J, et al. Dynamics of tumor and immune responses during immune checkpoint blockade in non-small cell lung cancer. *Cancer Res* 2019; **79**:1214−25.

11. Geng Z, Xiao Y, Zhu XJ, Ye C, Zhou JF. Anti-PD-1 therapy for clinical treatment of lymphoma: a single-arm meta-analysis. *Oncotarget* 2018;**9**:35343−55.

12. Heskamp S, Hobo W, Molkenboer-Kuenen JD, Olive D, Oyen WJ, Dolstra H, et al. Noninvasive imaging of tumor PD-L1 expression using radiolabeled anti-PD-L1 antibodies. *Cancer Res* 2015;**75**:2928−36.

13. Josefsson A, Nedrow JR, Park S, Banerjee SR, Rittenbach A, Jammes F, et al. Imaging, biodistribution, and dosimetry of radionuclide-labeled PD-L1 antibody in an immunocompetent mouse model of breast cancer. *Cancer Res* 2016;**76**:472−9.

14. Bensch F, van der Veen EL, Lub-de Hooge MN, Jorritsma-Smit A, Boellaard R, Kok IC, et al. [89]Zr-atezolizumab imaging as a non-invasive approach to assess clinical response to PD-L1 blockade in cancer. *Nat Med* 2018;**24**:1852−8.

15. Lesniak WG, Chatterjee S, Gabrielson M, Lisok A, Wharram B, Pomper MG, et al. PD-L1 detection in tumors using [^{64}Cu]atezolizumab with PET. *Bioconjugate Chem* 2016;**27**:2103−10.

16. Hettich M, Braun F, Bartholomä MD, Schirmbeck R, Niedermann G. High-resolution PET imaging with therapeutic antibody-based PD-1/PD-L1 checkpoint tracers. *Theranostics* 2016;**6**:1629−40.

17. Park HK, Kim M, Sung M, Lee SE, Kim YJ, Choi YL. Status of programmed death-ligand 1 expression in sarcomas. *J Transl Med* 2018;**16**:303.

18. Stühler V, Maas JM, Bochem J, da Costa IA, Todenhöfer T, Stenzl A, et al. Molecular predictors of response to PD-1/PD-L1 inhibition in urothelial cancer. *World J Urol* 2018;**37**:1773−84.

19. Guo X, Zhu H, Liu T, Xu X, Kong Y, Yao S, et al. Development of ^{99m}Tc-conjugated JS001 antibody for *in vivo* mapping of PD-1 distribution in murine. *Bioorg Med Chem Lett* 2019;**29**:2178−81.

20. Sun W, Yang Z, Lin H, Liu M, Zhao C, Hou X, et al. Improvement in affinity and thermostability of a fully human antibody against interleukin-17A by yeast-display technology and CDR grafting. *Acta Pharm Sin B* 2019;**9**:960−72.

21. Sheng X, Yan X, Chi Z, Si L, Cui C, Tang B, et al. Axitinib in combination with toripalimab, a humanized immunoglobulin G_4 monoclonal antibody against programmed cell death-1, in patients with metastatic mucosal melanoma: an open-label phase IB trial. *J Clin Oncol* 2019;**37**:2987−99.